Tuning Intermolecular Interactions: A Study of the Structural and Vibrational Properties of *p*-Hexaphenyl under Pressure

S. Guha,*,† W. Graupner,‡ R. Resel,§ M. Chandrasekhar,|| H. R. Chandrasekhar,|| R. Glaser,⊥ and G. Leising§

Department of Physics, Astronomy & Materials Science, Southwest Missouri State University Missouri 65804, Department of Physics, Virginia Tech., Blacksburg, VA 24061, Institut für Festkörperphysik, Technische Universität Graz, A-8010 Graz, Austria, Department of Physics & Astronomy, University of Missouri, Columbia, MO 65211, and Department of Chemistry, University of Missouri, Columbia, MO 65211

Received: December 20, 2000; In Final Form: April 9, 2001

Hydrostatic pressure is used to modulate the intermolecular interactions in the conjugated oligophenyl, *para*-hexaphenyl. These interactions affect the structural properties and also cause changes in the molecular geometry that directly alter the electronic properties. We use Raman spectroscopy to investigate the nature of the structural changes. Our Raman studies in the temperature range of 12 K to 300 K, under pressures up to 70 kbar, indicate that the potential energy of two neighboring phenyl rings as a function of the torsional angle is "W"-shaped. The libration of the phenyl rings between the two minima of the "W"-shaped potential can be modulated by either promoting the molecule to a higher energy state (activation energy of 0.045 eV) by raising the temperature or by decreasing the intermolecular separation, which makes the potential more "U"-shaped. Both these situations make the molecule seem more planar. We infer the shape of the potential from the relative intensity of the inter-ring C—C stretch Raman mode at 1280 cm^{-1} to the C—H bending mode at 1220 cm^{-1} (I_{1280}/I_{1220}). These results are interpreted within the framework of ab initio electronic and vibrational spectra calculations of a biphenyl molecule. We have also conducted X-ray studies to check the sample purity.

I. Introduction

The para-substituted oligophenyls have been found to be efficient blue laser dyes,[1] and the blue photoluminescence (PL) with a quantum yield of 30% has been the motivation for using *para*-hexaphenyl (PHP) as the emitting layer in organic light emitting diodes (LEDs).[2,3,4] By utilizing efficient color conversion techniques, the blue emitter PHP can be used to build red-green-blue LEDs.[5] The electronic properties of this class of materials have been predicted[6] and were found[7,8] to be highly anisotropic with respect to the molecular axis. The anisotropy in the emission process can be used to build LEDs with polarized emission,[9] which are of primary importance for backlighting applications in liquid crystalline displays. Though PL quantum yield is high enough for the use of PHP in LEDs and other devices, their properties still need to be improved for commercial applications.

Despite numerous efforts to understand the electronic properties of oligophenyls,[10] there are still unresolved questions regarding the *structure−property relations* concerning the arrangement of the phenyl rings *within* one molecule and the arrangement of the molecules *with respect to their neighbors*. The geometrical arrangement within one molecule and intermolecular interactions dramatically alter the optical and electronic properties of these materials.[11]

To understand the influence of intermolecular interactions on the electronic properties of oligo-and poly-*para*-phenylenes (PPP), several experiments have addressed this issue by studying the difference in PL quantum yields (PLQY) between films and solutions. For example, in methylated PPP (m-LPPP), the PLQY of solution and film are 100% and 30%, respectively.[12] Decyloxy PPP (DO PPP) exhibits a PLQY of 85% in solution and 35% in film.[13] These studies indicate that in the solid sate, intermolecular interactions alter the luminescent efficiencies. Recently, Cornil et al.[11] have reported a detailed correlated quantum-chemical calculation on interacting conjugated chains. They have shown how interchain coupling affects the electronic and optical properties with respect to those calculated for isolated chains.

In this work, we use hydrostatic pressure as the parameter that influences the intermolecular interaction. Pressure changes the intermolecular distances and tunes the structural and electronic properties of conjugated molecules without changing the chemical nature of the material. This technique is very different from changing the intermolecular interaction via chemical substitution, which typically introduces torsion in the polymer backbone.[14] We use Raman scattering to probe the geometry of a given molecule when it is affected by the increased proximity of the chains.

A theoretical approach by Rumi and Zerbi[15] shows that Raman intensities are a test bench for probing the change in the potential well between neighboring phenyl rings when oligo-*p*-phenylenes change from a nonplanar to a planar geometry. With a view toward understanding the structural properties, which in turn affect the electronic properties, our Raman scattering studies of PHP under hydrostatic pressure provide

* To whom correspondence should be addressed. E-mail: sug100f@smsu.edu.
† Department of Physics, Astronomy & Materials Science, Southwest Missouri State University.
‡ Dept. of Physics, Virginia Tech., Blacksburg.
§ Institut für Festkörperphysik, Technische Universität Graz.
|| Department of Physics & Astronomy, University of Missouri.
⊥ Department of Chemistry, University of Missouri.

10.1021/jp0045540 CCC: $20.00
Published on Web 05/25/2001

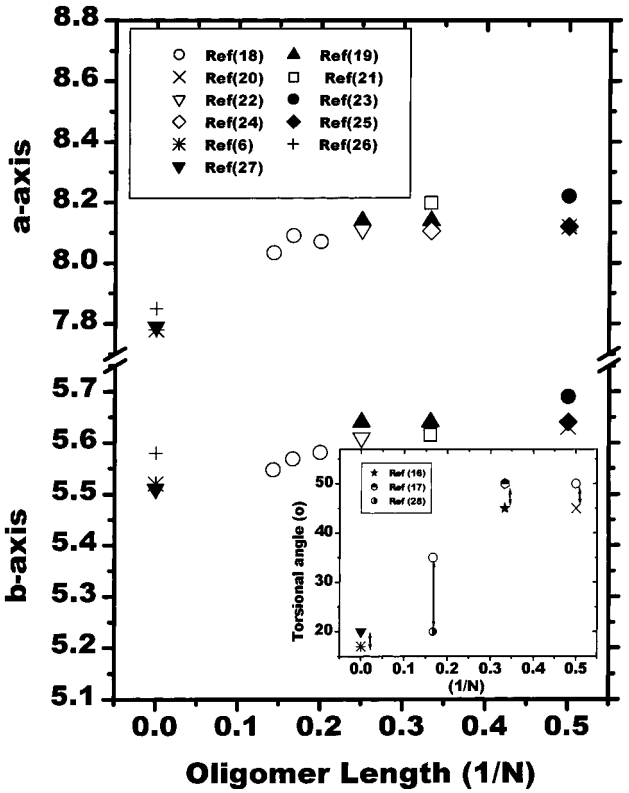

Figure 1. The lattice constants of oligophenyl crystals (a and b) vs 1/oligophenyl length. Increase in the oligophenyl length decreases the lattice constants. This is a compilation of data from ref 6 and refs 18−28. The inset shows the calculated torsional angle between neighboring phenyl rings as a function of 1/oligophenyl length from various theoretical calculations (refs 6, 16−18, 20, 27, and 28).

an independent tool for studying the torsional angles between neighboring phenyl rings. In our experiments, we see the effect of two mechanisms; increasing intermolecular interaction caused by bringing the molecules closer together, and simultaneous effect of changing the geometry of the molecules. Raman intensities, in particular the ratio of the intensity of the C—C stretch mode at 1280 cm^{-1} to the C—H in-plane bending mode at 1220 cm^{-1} (I_{1280}/I_{1220}) provide insight into the torsional angle between two neighboring phenyl rings.

Our experiments indicate that the potential energy of two neighboring phenyl rings versus the torsional angle is "W"-shaped, changing to a "U"-shape by application of pressure. Previous work comparing isolated molecules versus crystals shows that the "W"-shaped potential becomes narrower, i.e., the minima are brought closer in the crystalline form owing to the intermolecular forces. A torsional angle of 27° is predicted in single isolated PPP chains and 17° in the crystalline environment.[6] Similarly, the oligomer length is also related to the torsional angle, which is predicted by molecular simulations: inter-ring torsional angles of approximately 45°−50° for biphenyl and terphenyl,[16,17] 30°−40° for hexaphenyl[18] and 27° in single isolated PPP chains.[6]

Conventional X-ray probes the lattice structure but does not give the geometrical orientation of the basis. Rietveld refinement is complicated in these materials due to texture effects and therefore an accurate estimate of the torsional angle between phenyl rings is difficult when solely based on X-ray measurements.

Figure 1 shows a compilation of experimental X-ray data for the oligophenyls of PPP.[6,18−27] Refs 6, 26, and 27 are for a PPP chain. It is observed from Figure 1 that upon increasing the oligophenyl length, the lattice constants *a* and *b* perpendicular to the chain direction decrease, increasing the crystallographic packing in the *ab*-plane. Because molecular simulations show that the torsional angles decrease upon closer packing, increasing the oligomer length decreases the torsional angles as shown in the inset of Figure 1. The values of the torsional angles are from various works (refs 6, 16−18, 27, and 28). Though the torsional angles are based on different theoretical approaches, it is nevertheless interesting to note the trend that increasing the chain length decreases the torsional angle between neighboring phenyl rings.

This paper is organized as follows: We first present the experimental X-ray studies of PHP. This is followed by the experimental Raman scattering results of PHP as a function of temperature and hydrostatic pressure. We discuss the issue of planarization of the molecule based on our experimental results. To theoretically describe the effect of planarization on the Raman spectrum of oligophenyls, we calculated the Raman spectrum of a smaller molecule, namely biphenyl for planar and nonplanar geometries using the restricted Hartree−Fock method. The theoretical methodology and results are presented in the last section.

II. Experimental Section

The PHP powder was obtained from Tokyo Chemical Industries Ltd. The X-ray diffraction pattern was measured with a SIEMENS D501 powder diffractometer. Ni-filtered Cu Kα radiation was used and the PHP powder was deposited on a nonreflecting monocrystalline silicon substrate. Raman measurements were carried out in a backscattering configuration, using the 514.5 nm line of an Ar^+ laser. The scattered light was detected with a SPEX triple monochromator equipped with a CCD array detector and a holographic supernotch filter. Pressure studies were conducted in a Merrill−Bassett type diamond anvil cell (DAC) with cryogenically loaded argon as the pressure medium. Pressure (P) was measured via the luminescence of a ruby chip located in the pressure chamber. Temperature was varied by mounting the DAC in a closed cycle helium refrigerator.

III. Crystal Structure of *para*-Hexaphenyl

III.1. Three-Dimensional Structure of PHP. Organic molecules have received renewed attention with recent advances in organic crystal growth technique, which now enables organic optoelectronic devices, such as the solid-state injection laser.[29] In this respect, PHP, which has a very well-defined chain length, and high PLQY has tremendous potential in the field of organic optoelectronic devices. The conformations of polyphenyls, in solution and in molecular crystal, significantly affect the optical properties. There have been numerous studies on the crystal structure of the oligophenyls of PPP, starting with the determination of the structure of biphenyl in the late nineteen twenties.[23,30] The crystal structures of all oligophenyls from biphenyl to heptaphenyl have been investigated in detail via single-crystal studies. Within this series of oligophenyls, the arrangement of the molecules in the crystal structure is similar. In the crystalline state, the molecules are arranged in layers, where the chains are stacked in a way such that the molecular planes are non-coplanar. Within the classification of polynuclear aromatic hydrocarbons, this type of structure is of the herringbone type.[31,32] The long axes of the molecules are nearly perpendicular to the layers, and therefore, the thickness of a layer is approximately the length of the molecule.

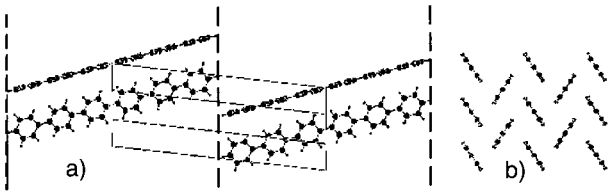

Figure 2. (a) The unit cell and the position of the PHP molecules relative to the unit cell which connects two layers of PHP. (b) The herringbone arrangement of the PHP molecules within one layer.

Early attempts to determine the structure of PHP ($C_{36}H_{26}$) were done by X-ray powder patterns and by Weissenberg photographs.[33,34] The results are in reasonable agreement with single-crystal investigations performed by using a four circle goniometer: PHP has a monoclinic unit cell, space group $P2_1/a$ with $a = 8.091$ Å, $b = 5.568$ Å and $c = 26.24$ Å, and the monoclinic angle $\beta = 98.17°$.[18] The distances between the C atoms vary between 1.322 and 1.507Å, consistent with the value of 1.41Å expected for aromatic bonds of carbon.[35] The distances between a C atom and the adjacent H atom are determined as 0.95Å in comparison with the expected distance of 1.08Å.[33]

A schematic diagram of the crystal structure of PHP is shown in Figure 2. The positions of the atoms are taken from ref 18. The large circles represent carbon atoms and the small circles represent hydrogen. The unit cell is represented by the long dashed lines and the layers are indicated by short dashed lines in Figure 2a. The long axis of the unit cell (*c*-axis) connects two layers of PHP molecules and each layer is represented by two molecules. The plane of the two short crystallographic axes of the unit cell (ab-plane) is parallel to the PHP layers. The monoclinic angle β is determined by the relative position of two PHP molecules of neighboring layers, which are in the same orientation, i.e., the angle of the ab-plane with the *c*-axis. The arrangement of the molecules within one layer is shown in Figure 2 (b).

Owing to the single bond between neighboring phenyl rings these rings show torsional motion. These torsions cause large Debye−Waller factors in the carbon atoms, which are not situated along the long axis of the molecule.[18] The nature of the torsional motion of the neighboring phenyl rings is determined by at least two influences: (1) *intramolecular repulsion* between ortho hydrogen and (2) the tendency toward planarization in a π-electron system due to the resonance interaction.[36] Simulations of crystalline packed PHP show a movement of the phenyl rings in a symmetrical potential where the amplitude of the torsions is approximately[28] $\pm 20°$.

III.2. Phase Determination. The phase purity of the PHP sample was checked by X-ray scattering studies. An X-ray powder pattern of the material is shown in the top panel of Figure 3; the lower panel shows the calculated powder pattern, and gives information about position and intensity of the X-ray reflections. The calculation is based on single-crystal data[18] using the program POWDER CELL.[37] The agreement of the experiment with the calculation and other experimental powder patterns is quite good,[38] although (001) reflections are overemphasized. This can be explained by a preferred orientation of the anisotropic PHP crystallites in the powder because they are disk shaped in the (001) plane.

Small traces of another crystalline phase are found in the powder spectrum of the PHP sample as shown in Figure 4. This impurity is identified as the metastable high-temperature polymorph of PHP. The position and intensity of the X-ray reflections of the solved phase as well as of the high-temperature polymorph are given by filled and open bars, respectively, at

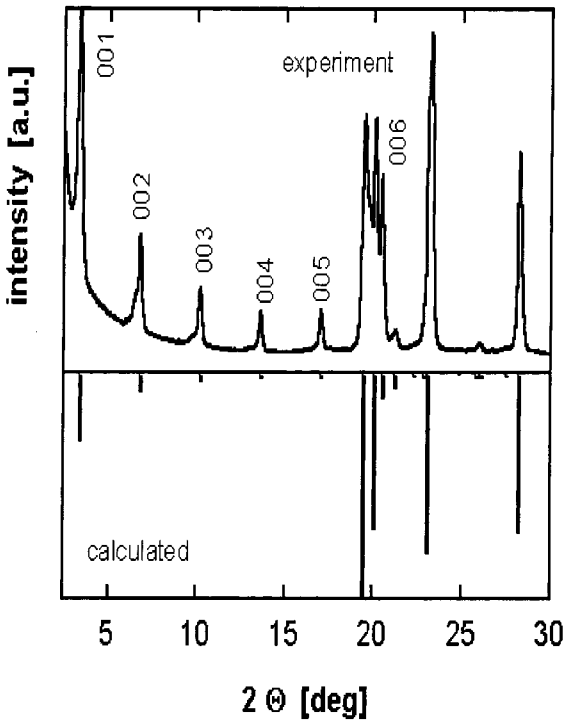

Figure 3. Experimental X-ray powder pattern of PHP (top) and calculated pattern (bottom). The full bars give the position as well as the relative intensity of the X-ray reflections.

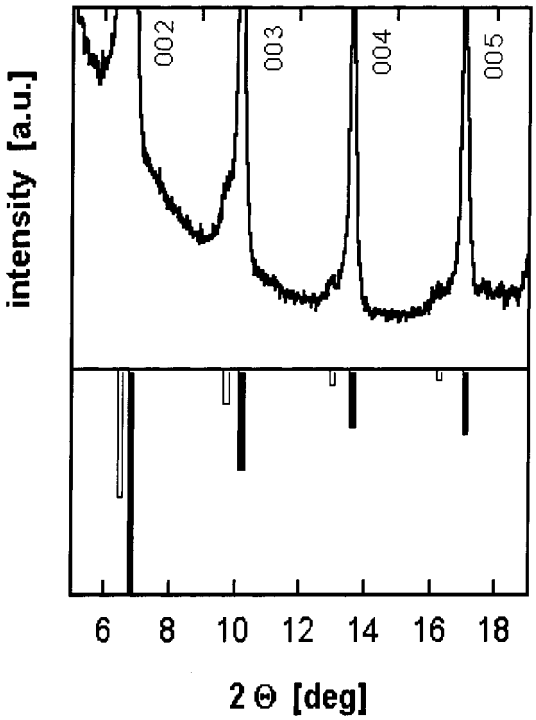

Figure 4. Phase analysis of the experimental powder pattern in the range of 5°−19° (top) reveals small traces of a high-temperature polymorph of PHP which is designated by open bars (bottom).

the bottom panel of Figure 4. The packing of the PHP molecules in the high-temperature phase is also a herringbone structure as is the solved one[39] with the layer thickness being slightly larger.

IV. Raman Spectrum of *para*-Hexaphenyl − Experimental Results

The Raman spectrum of the oligophenyls has been described by several authors [40−45] and is mainly characterized by four

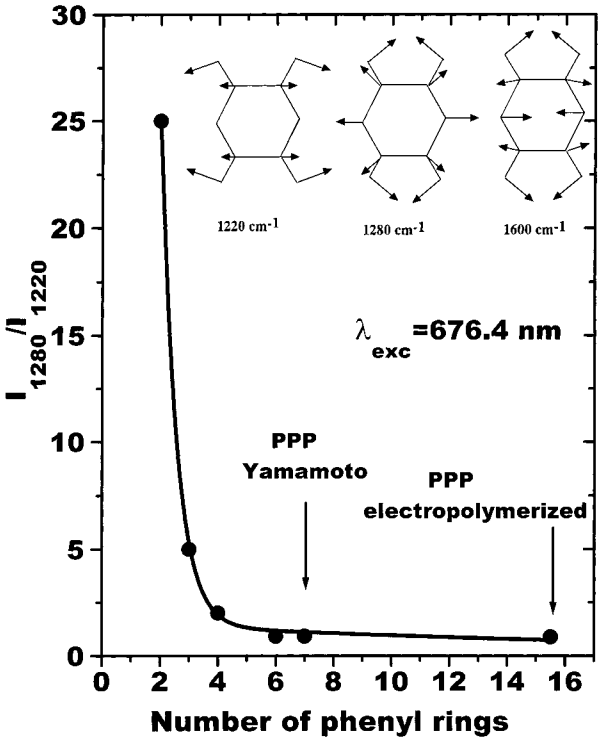

Figure 5. I_{1280}/I_{1220} vs conjugation length N (ref 46) for several oligophenyls and $N = 7$ is from ref 47. The inset shows the mode displacement pattern of three nondegenerate Raman modes in PHP.

intense modes of A_g symmetry. The mode displacement pattern for three of these modes is shown in the inset of Figure 5. It has been observed that the ratio of the Raman intensities I_{1280}/I_{1220} is a good indication for number of phenyl rings in the molecule,[41,42,46] and consequently a test for planarity because simulations show that a higher number of conjugated phenyl rings results in a lower torsional angle between the phenyl rings (inset of Figure 1). Doping, which is redox reaction of a chemical agent with the oligophenyl resulting in a charge-transfer process also results in lowering the I_{1280}/I_{1220}. This can be explained by the more quinoid structure of the doped oligophenyl, which is accepted to be more planar than the neutral benzoid ground state.[47] Raman scattering of the *anions* of the oligophenyls (from *p*-terphenyl up to *p*-hexaphenyl) also shows that I_{1280}/I_{1220} decreases as the oligophenyl length is increased.[42] For a biphenyl molecule, $I_{1280}/I_{1220} \approx 25$; beyond six phenyl rings the ratio of the intensities is close to unity, as shown in Figure 5. The values for I_{1280}/I_{1220} in Figure 5 are from ref 46, except for the value of I_{1280}/I_{1220} for 7 phenyl rings, which is from ref 48.

IV.1. Temperature Effects. Figure 6 shows a typical Raman spectrum of PHP at 1 bar for two different temperatures. The ring C—C stretch mode at 1600 cm^{-1} is observed in addition to the 1220 and 1280 cm^{-1} modes. We find that as temperature is decreased to 12 K, the integrated intensity of the inter-ring C—C stretch mode at 1280 cm^{-1} increases with respect to the C—H in-plane bending mode at 1220 cm^{-1} as shown in Figure 7. The open circles and the solid squares are the experimental results with the 647.1 nm and the 514.5 nm line as the excitation sources, respectively. Note that the 647.1 nm line is far from resonance in PHP. The temperature behavior of I_{1280}/I_{1220} is indicative of a smaller torsional angle observed at room-temperature changing to larger torsional angle, (more nonplanar geometry) at lower temperatures, similar to what is observed in lower polyphenyls.[49,50,51] The bold line in Figure 7 is a fit to a functional described below.

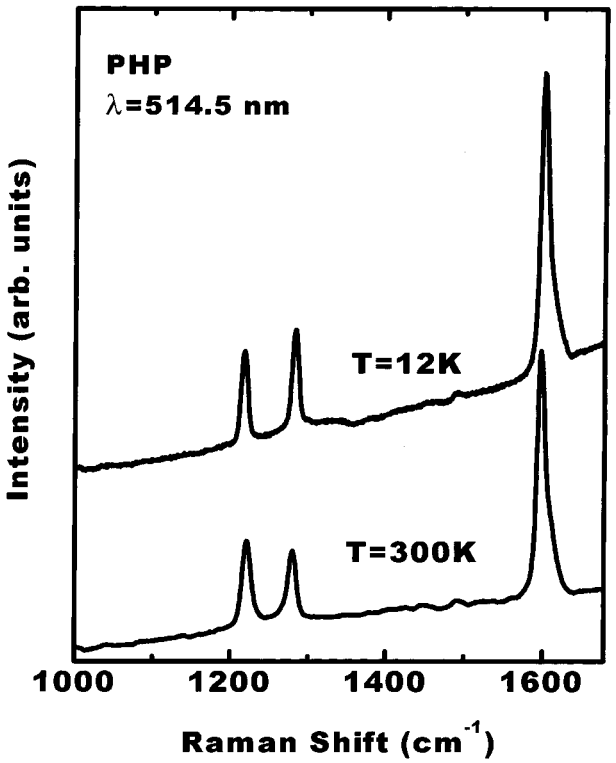

Figure 6. Raman spectra of PHP at ambient pressure and at 12 K and 300 K.

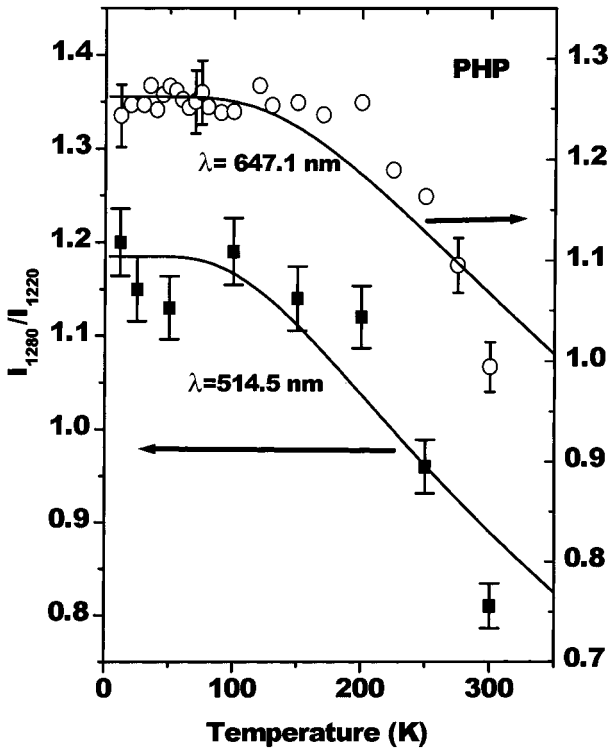

Figure 7. Ratio of the intensity of the 1280 cm^{-1} mode to the 1220 cm^{-1} mode in PHP as a function of temperature for two different excitation wavelengths: near resonance at 514.5 nm and off-resonance at 647.1 nm. The bold line is a fit to the functional form $A^*(1 - \exp(-\Delta E_{np\rightarrow p}/k_BT))$ and the symbols are the experimental results.

The temperature-dependent Raman studies require that the functional dependence of the potential energy of two neighboring phenyl rings vs torsional angle is "W"-shaped[21,52] as depicted in Figure 8. The Raman spectra of PHP vs temperature show a pronounced change in I_{1280}/I_{1220} (Figures 6 and 7). From Raman

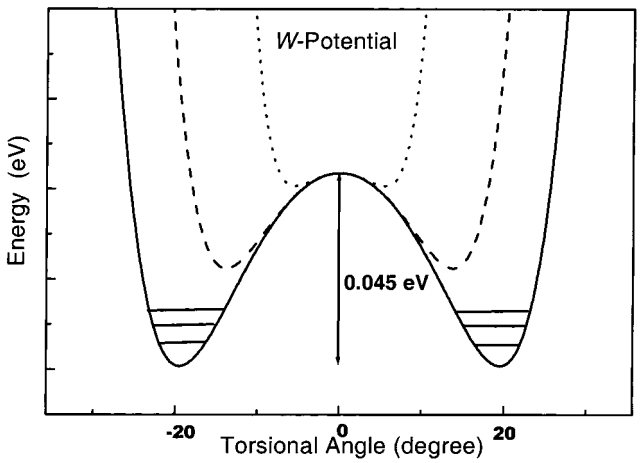

Figure 8. Schematic of the potential energy curve between two neighboring phenyl rings vs torsional angle in PHP. The thick bold line represents the potential at ambient pressure whereas the dashed and the dotted line represent the potential energy curve at higher pressures. The angle corresponding to the minimum in potential energy is chosen in accordance with ref 28; the well depth is derived from our experiment.

studies on oligophenyls of different length, it is known that I_{1280}/I_{1220} decreases with increasing chain length (Figure 5). At the same time, the torsional angle between phenyl rings decreases with increasing chain length (see Figure 1). Therefore, I_{1280}/I_{1220} can be used as an indicator for planarity in these materials—a higher I_{1280}/I_{1220} corresponds to a lower planarity. Lowering the temperature leads to an increase of I_{1280}/I_{1220} which implies a decrease in planarity. The I_{1280}/I_{1220} versus temperature data (Figure 7) shows a behavior typical of a thermally activated process described by Boltzmann statistics. Thermal energy is required in order to populate a higher lying level corresponding to the planar conformation of the molecules. This level is characterized by the expectation value $\langle \psi \mid \phi \mid \psi \rangle$ for the angle-operator ϕ, which becomes 0 instead of $\pm\delta$ at the minima of the potential shown in Figure 8. The probability for the system to be in a nonplanar configuration is proportional to I_{1280}/I_{1220}. Therefore, we subtract the Boltzmann term, which is proportional to the probability of finding the PHP molecule in a planar configuration, from unity. We fit the data to

$$I_{1280}/I_{1220} = A \times (1 - exp(-\Delta E_{np\rightarrow p}/k_B T)) \qquad (1)$$

where k_B is Boltzmann's constant, $\Delta E_{np\rightarrow p}$ is the difference in energy between the nonplanar ground state and the planar state reachable via thermal excitation. By fitting I_{1280}/I_{1220} versus temperature to eq 1, we obtain an activation energy of $\Delta E_{np\rightarrow p} = 0.04 \pm 0.003$ eV with the 514.5 nm line and $\Delta E_{np\rightarrow p} = 0.05 \pm 0.003$ eV with the 647.1 nm line. Because the activation energies are similar to the two different excitation lines (near resonance and off-resonance conditions) the conformational changes are not a function of any resonance mechanism.

The average value of $\Delta E_{np\rightarrow p} = 0.045$ eV for PHP is reasonable when compared to that of a biphenyl molecule. In section V, we calculate $\Delta E_{np\rightarrow p}$ from the difference in internal energy between the planar and nonplanar configuration of a biphenyl molecule. For biphenyl the nonplanar configuration reaches its minimum energy when the phenyl rings are tilted at an angle of 52° with respect to each other. Table 1 summarizes our results. The restricted Hartree−Fock method gives a slightly higher value for $\Delta E_{np\rightarrow p}$ compared to the density functional method. It is not surprising that the calculated values for the biphenyl are higher: the torsional angle ($\pm\delta$) for the phenyl rings of a biphenyl molecule and for the PPP single chain is higher than that for the PHP crystal indicating a steeper potential well (Figure 8). We thus conclude that increasing the temperature does not change the actual shape of the potential energy curve but promotes the molecule to a higher energy state which is the more planar configuration. Our theoretical calculations of the activation energies are consistent with other ab initio calculations of the biphenyl molecule.[53,54]

TABLE 1: Calculated and Experimental Energies of Short Oligophenyls[a]

structure	$\Delta E_{np\rightarrow p}$ (eV)
biphenyl (RHF)	0.145
biphenyl (B3LYP)	0.089
PPP chain[b]	0.065
PHP (expt)	0.045 ± 0.003

[a] The first two rows are the results of our calculation for a biphenyl molecule using restricted Hartree−Fock with a polarized basis set 6−31 G* within the density functional theory. The second column shows the activation energy in going from a non-planar to a planar geometry. The activation energy for PHP has been calculated from Figure 7. [b] Ref 6.

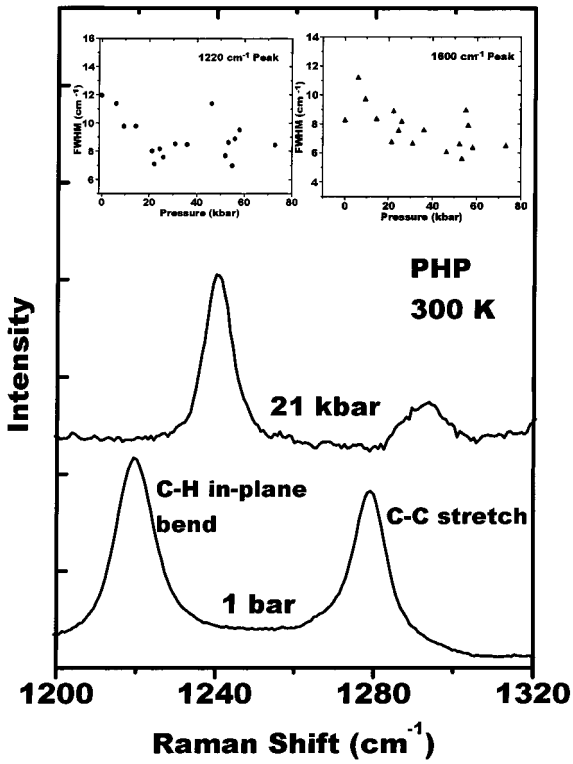

Figure 9. Raman spectra of PHP at 1 bar and 21 kbar, at 300 K. The inset shows the line broadening parameter (fwhm) for the 1220 cm^{-1} and the 1600 cm^{-1} Raman modes as a function of pressure.

IV.2. Pressure Effects. Although temperature affects the population of the higher-lying (more planar) states, pressure increases the proximity of the molecules. The most striking feature of the Raman spectrum of PHP is the decrease in the intensity of the 1280 cm^{-1} peak relative to the 1220 cm^{-1} peak, (I_{1280}/I_{1220}) at high pressures (and room temperature) as shown in Figure 9. Figure 10 shows the ratio of the integrated intensities, I_{1280}/I_{1220} as a function of pressure. At 1 bar the ratio of the intensities is 0.84 and at higher pressures beyond 15 kbar, the average value of I_{1280}/I_{1220} is 0.3. The solid line is a guide to the eye. This decrease in intensity of the inter-ring C−C stretch mode at higher pressures is due to the planarization of the molecule.

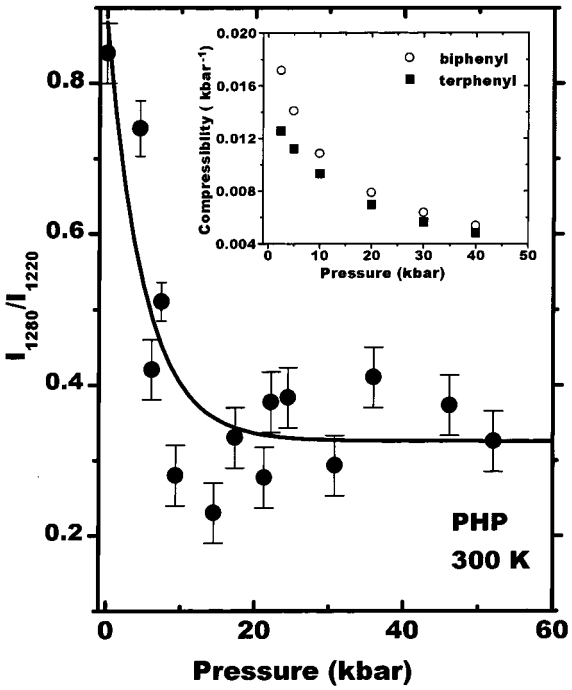

Figure 10. Ratio of the intensity of the 1280 cm^{-1} mode to the 1220 cm^{-1} mode as a function of pressure at $T = 300$ K. The solid line is a guide to the eye. The inset shows the compressibility of biphenyl and terphenyl vs pressure from ref 57.

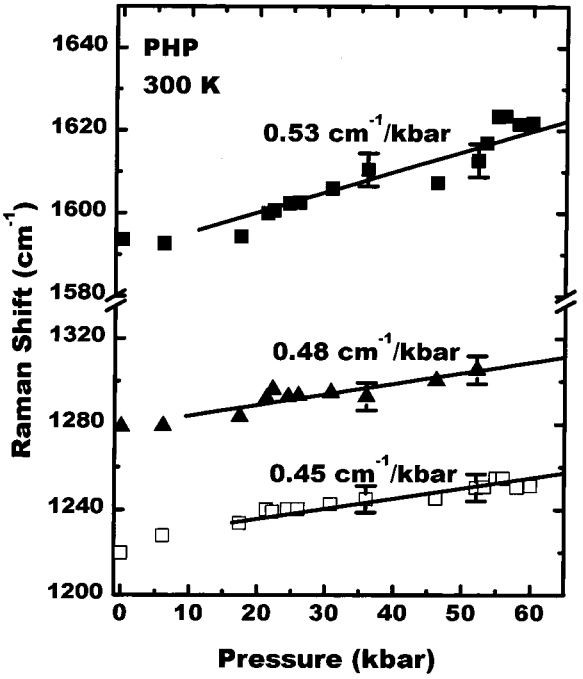

Figure 11. Raman frequencies of the C—H bending mode at 1220 cm^{-1}, C—C stretch mode at 1280 cm^{-1}, and C—C stretch mode at 1600 cm^{-1} as a function of pressure. Typical error bars are shown for a few data points. These measurements are at $T = 300$ K and the linear fit is above 15 kbar.

The weaker bonds in the a−b direction bring the molecules closer, thus increasing their intermolecular interaction. These interactions have a profound effect on the potential energy curve of the Raman modes of the molecule. The Raman intensities under hydrostatic pressure shed light on the torsional angle of the phenyl rings. Upon increasing pressure the "W" shape of the potential energy curve changes; it becomes narrower, starts losing the "W" shape, and becomes more "U" like as shown schematically by the dashed and the dotted lines in Figure 8. This in turn means that the energetic difference ($\Delta E_{np\rightarrow p}$) between the nonplanar and the planar conformation of the molecule decreases with increasing pressure. Our experiment completely confirms the model. The ratio of I_{1280}/I_{1220} decreases from 0.8 to 0.3 between 0 and 15 kbar, beyond which the ratio remains almost a constant (Figure 10). Furthermore, changing the temperature from 10 to 300 K at 20 kbar does not result in any change of I_{1280}/I_{1220} indicating that maximum planarity between the neighboring phenyl rings is reached.

We have measured the three Raman modes as a function of pressure. The frequencies of all modes increase linearly with pressure beyond 15 kbar and are fit to $\omega(P) = \omega(0) + (d\omega/dP)xP$, where P is in kbar. A Lorentzian curve fitting routine was used to determine the frequencies of the Raman modes. The mode frequencies as a function of pressure are shown in Figure 11. These measurements were all performed at 300 K. The linear fit is only beyond 15 kbar. At lower pressures the slopes seem to be somewhat different because of the nonplanar geometry of the molecule and this region is being investigated with greater detail. All the three Raman modes have similar pressure coefficients. On increasing the pressure beyond 60 kbar, the 1280 cm^{-1} mode interferes with the Raman mode from diamond of the anvil cell at 1333 cm^{-1}. The linearity of the Raman modes versus pressure is also observed in the work by Webster and Batchelder, in which they have measured the Raman spectra of poly(*p*-phenylenevinylene) under pressure.[55]

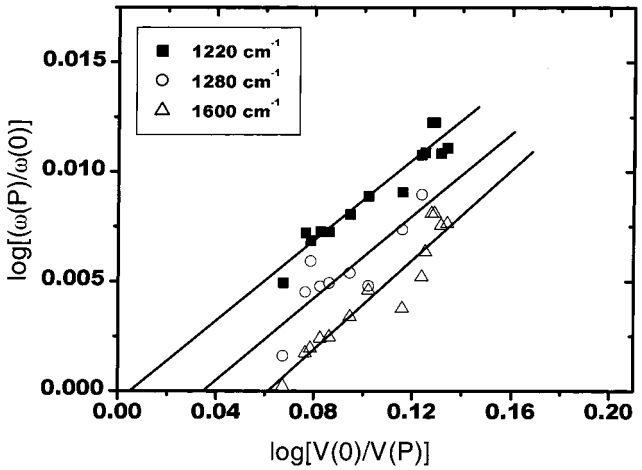

Figure 12. A log−log plot of the wavenumber ratio $\omega(P)/\omega(P)$ Vs. the volume ratio $V(0)/V(P)$ for the 1220 cm^{-1}, 1280 cm^{-1}, and the 1600 cm^{-1} modes in PHP, beyond 15 kbar. The volume ratio is obtained from the compressibility of *p*-terphenyl.

Pressure-induced vibrational frequency shifts in a bulk crystal are often characterized by

$$\frac{\omega_i(P)}{\omega_i(0)} = \left[\frac{V(0)}{V(p)}\right]^{\gamma_i} \qquad (2)$$

where $\omega_i(P)$ is the wavenumber of the ith mode at the applied pressure P, $V(P)$ is the volume of the bulk solid at pressure P, and γ_i is a vibrational mode Grüneisen parameter.[56] Because the bulk modulus and the volume dependence under pressure are not know for PHP, we estimate the Grüneisen parameter from eq 2 by using the change in volume under pressure for *p*-terphenyl.[57] Figure 12 shows a plot of $\log[\omega(P)/\omega(0)]$ versus the change in volume under pressure for the three Raman modes in PHP, beyond 15 kbar. Using a linear fit for all the three

modes, it can be clearly seen that none of the fits go through the origin, as one would have expected if eq 2 were valid. Linear regression analysis for all three lines in Figure 12 (where the intercepts are nonzero) yield a value of ~0.09 for the slope. The deviation from eq 2 does not arise from the fact that we use the *p*-terphenyl data for $\log[V(0)/V(P)]$ because the intercepts for the 3 modes are different; a simple rescaling is different for all the three lines. This implies that the three Raman modes have different compressibilities associated with them. To simulate pressure effects, recent calculations of absorption in PPP show that changing the perpendicular distance between chains has a much stronger effect on the broadening as well as the energy positions compared to changing the in-plane interchain distance.[58] Therefore, it is not very surprising that the volume ratio $V(0)/V(P)$ is different for the three Raman modes.

The volume compressibility is dependent on pressure (see inset of Figure 10). At 40 kbar, the pressure dependent volume decrease is approximately[57] 20% which implies that the lattice constants change by almost 7% on the average. For PHP, we expect similar volume changes with pressure. Our experiments show that the pressure dependence of the Raman modes is linear beyond 15 kbar once the molecule is planarized (Figure 11). The atomic displacement (inset of Figure 5) for the three modes takes place primarily *along the chain direction*. Therefore, the observed linearity of frequency versus pressure indicates that the lattice constant *along the chain* also changes linearly with pressure. The compressibility *along the chain direction* is not affected by pressure. Therefore, the pressure dependent part of the compressibility in biphenyl and terphenyl must be due to effects along the *a*-and *b*-axes, which are perpendicular to the chain axis. This is also supported from recent calculations.[58] Furthermore, planarization of the phenyl rings would also contribute to further increasing the compressibility in the $a-b$ direction. Interestingly enough, a steep drop in compressibility occurs in the low-pressure region, which is the same pressure range in which the Raman data of PHP (Figure 10) shows the effect of planarization. Using the average bulk modulus of terphenyl (67 kbar) and the unit cell parameters for PHP, we calculate the average energy stored per PHP molecule due to a volume change at a pressure of 10 kbar to be 0.54 eV. This corresponds to a maximum energy of 0.1 eV connecting a single bond, much higher than the activation energy needed for planarization. It is therefore reasonable to expect that at 10 kbar all the molecules be planarized.

Furthermore, our observations indicate that all the phenyl rings of a PHP molecule are planarized to the same extent. The evidence of this conclusion comes from the observation that there is little broadening of the Raman modes as a function of pressure beyond 15 kbar (inset of Figure 9). Broadening of Raman lines, in particular the ring C—C stretch mode at 1600 cm^{-1} in PHP is typical for samples consisting of different conjugation lengths.[59] The Raman modes, we observe, are from a similar distribution of conjugation lengths both under pressure and at 1 bar. This excludes the possibility that pressure only affects certain isolated rings because that would produce a broader distribution of conjugation lengths. Though the Raman experiments probe the intramolecular modes, the planarization of the phenyl rings is a consequence of the increased *intermolecular* interaction by the application of high pressure.

V. Theory

V.1. Methodology for Electronic and Vibrational Structure Calculations. To obtain a quantitative estimate of the changes in the Raman spectrum due to planarization, we calculated the spectrum for a biphenyl molecule in a planar form and with the phenyl rings tilted at 52°, which is the minimum energy condition for the molecule. We employed the restricted Hartree−Fock (RHF) method[60] to perform geometry optimizations, force constant calculations, and dipole moment/polarizability derivatives with a polarized basis set 6-31G* for a biphenyl molecule.[61] Geometry optimization and total energy calculations of the system were also done using Becke's Three Parameter Density Functional Hybrid Method (B3LYP).[62] The Raman spectrum calculations are done in two steps; first the force constant matrix is evaluated and then the eigenvalue equation is solved to obtain the eigenvalues and eigenvectors. The Raman scattering activities are proportional to the polarizability derivatives taken with respect to the Cartesian coordinates. For a system of N atoms interacting via harmonic forces, the normal-mode frequencies $\{\omega_f\}$ and amplitudes $\chi(f)$ of mode f, where $f = 1,.....,3$ N labels the normal modes, are determined by a 3N × 3N matrix eigenvalue equation

$$(\Phi - \omega_f^2 \mathbf{M})\chi(f) = 0 \tag{3}$$

where Φ is the harmonic force constant matrix, and **M** is the mass matrix. Both the force constant and the mass matrices are symmetric. In the harmonic approximation, the intensity of off-resonance first-order Stokes scattering is given by

$$I_{\eta\eta} \propto \omega_L \omega_S^3 \sum_{f=1}^{3N} \frac{\langle n(\omega_f) + 1\rangle}{\omega_f} |\sum_{\alpha\beta} \eta_\alpha \eta_\beta P_{\alpha\beta,f}|^2 \times \delta(\omega - \omega_f) \tag{4}$$

ω_L and ω_S are the incident and scattered light frequencies; $\omega/\omega_L - \omega_S$ is the Raman shift; η and η' are unit vectors along the incident and scattered polarization direction, respectively; $\langle n(\omega_f)\rangle \equiv [\exp(\beta\hbar\omega_f) - 1]^{-1}$ is the thermal average occupation number of mode f at temperature $T = (k_B\beta)^{-1}$. $P_{\alpha\beta,f}$ is the derivative of the electronic polarizability tensor with respect to the normal coordinate of mode f; α and β are Cartesian coordinates. The Gaussian program calculates the Raman activities, which are given by the square of the polarizability tensor in the above expression. To obtain the Raman intensities, one has to multiply by the appropriate prefactors shown in eq 4.

The planar and the nonplanar biphenyl molecules were optimized with appropriate symmetry restrictions, i.e., D_{2h} and D_2 symmetries, respectively. It is known that ab initio self-consistent methods overestimate force constants because of which empirical scaling factors are introduced for the calculation of vibrational spectra.[41,63,64] This scaling alters the vibrational frequencies but does not affect the Raman and infrared intensities.[65] In our calculation, we do not use scaling factors since we are interested mainly in the ratio of the intensities of the inter-ring C—C stretch mode to the C—H bend mode.

V.2. Raman Intensity Calculations. Figure 13 shows the calculated Raman intensities for the biphenyl geometries in the nonplanar form where the two phenyl rings are tilted by an angle of 52° and in the planar form. Because the nonplanar geometry has a lower symmetry there is a greater number of Raman modes which get activated. The Raman frequencies are about 8% larger than the experimental values. Experimentally, for a (nonplanar) biphenyl molecule, [46] $I_{1280}/I_{1220} = 25$; from Figure 13, we find that the calculation for the nonplanar geometry yields $I_{1280}/I_{1220} = 14.5$. In the calculation for the planar geometry I_{1280}/I_{1220} decreases to 3.2. In comparing these theoretical results of the biphenyl molecule to our experimental results on PHP, we have

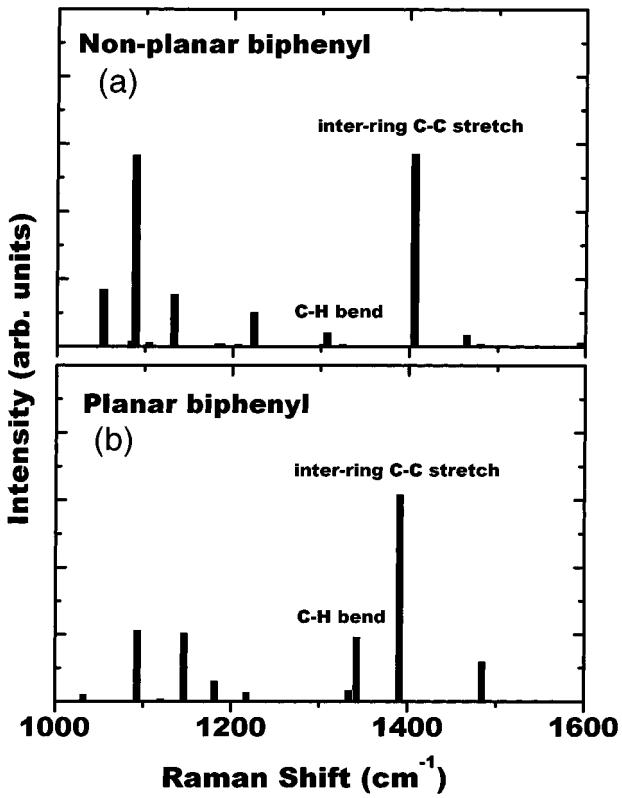

Figure 13. Calculated intensities of the Raman-active modes between 1000 and 1600 cm^{-1} region in a biphenyl molecule. (a) Raman intensities for a biphenyl molecule where the phenyl rings are nonplanar at an angle of 52° with a D_2 symmetry. (b) Raman intensities for a planar biphenyl molecule with a D_{2h} symmetry.

TABLE 2: Calculated and Observed Raman Intensities for Nonplanar and Planar Oligophenyls[a]

structure	I_{1280}/I_{1220} (nonplanar)	I_{1280}/I_{1220} (planar)	factor (nonplanar to planar geometry change)
biphenyl	14.5	3.2	4.5
PHP (expt)	0.84	0.3	2.8

[a]The biphenyl results are from our theoretical calculations and the PHP results are experimental. The second and the third columns give the ratio of the Raman intensity of the 1280 cm^{-1} mode to the 1220 cm^{-1} mode for the nonplanar and planar geometry, respectively. The last column gives the factor by which the ratio of I_{1280}/I_{1220} changes between the nonplanar geometry and the planar geometry. For PHP, the nonplanar geometry corresponds to the 1 bar case and the planar geometry corresponds to higher pressures.

to compare the ratio of I_{1280}/I_{1220} for the nonplanar geometry to the planar geometry. These results are summarized in Table 2. Experimentally, the nonplanar geometry corresponds to the 1 bar case and the planar geometry corresponds to higher pressures. For PHP, we measured $I_{1280}/I_{1220} = 0.84$ at 1 bar and an average value of 0.3 at higher pressures. Therefore, the experimentally obtained ratio of the intensities of the nonplanar geometry to the planar geometry is 2.8 (=0.84/0.3) for PHP which is quite close to the calculated value of 4.5 (=14.5/3.2) for the biphenyl case.

Our experimental results are also consistent with the scaled quantum mechanical oligophenyl force field (SQMOFF) vibrational spectra calculations by Cuff and Kertesz.[41] They have calculated the Raman Spectrum of PPP for two different geometries, (a) planar and (b) helical. For the planar geometry, it is observed that $I_{1280}/I_{1220} \sim 0.2$ close to our experimental value of 0.3 for the sample (PHP) under high pressure. The helical geometry on the other hand has a much higher value of I_{1280}/I_{1220} compared to the planar geometry.

VI. Conclusions

We have conducted a Raman scattering study on PHP where we vary the temperature and hydrostatic pressure. From a study of the relative intensities of the C—C stretch and the C—H in plane bend modes (I_{1280}/I_{1220}), we gain insight onto the torsional angles between phenyl rings and use the power of pressure to tune intermolecular interaction. We predict a "W"-shaped potential between neighboring phenyl rings as a function of torsional angle. Our experiments show that there are two ways of reaching a more planar configuration (a) via promotion of the molecule into a higher energy state by increasing the temperature (activation energy = 0.045 eV) and (b) via changing the shape of the potential from a "W"-shape to a "U"-shape by increasing pressure. The latter effect saturates around 15 kbar.

Our analysis of the linearity of the frequency of the Raman modes beyond 15 kbar indicate that much of the compression of the unit cell with pressure occurs in the $a-b$ plane, bringing the molecules closer together. The increased intermolecular interaction acts to planarize the molecules. In the process, all the molecules appear to be planarized to the same extent as evidenced from the unchanged broadening in the 1600 cm^{-1} mode.

The experimental intensity ratio I_{1280}/I_{1220} decreases by a factor of 2.8 when the PHP molecule goes from a nonplanar to a planar geometry. The ab initio calculations of the smaller biphenyl molecule indicate a change of a factor of 4.5. This close agreement corroborates our argument.

Acknowledgment. We acknowledge the financial support of U.S. Army DAAL03-92-0381, University of Missouri Research Board and *Oesterreichische Nationalbank* (project 6608). We would like to thank Q. Cai and C. Martin for their invaluable help in the laboratory. Useful discussions with C.A. Ullrich are acknowledged.

References and Notes

(1) Furumoto, H. W.; Ceccon, H. L. *IEEE J. Quantum Electronics* 6 **1970**, 262.

(2) Hosokawa, C.; Higashi, H.; Kusumoto, T. *Appl. Phys. Lett.* **1993**, *62*, 3238.

(3) Graupner, W.; Grem, G.; Meghdadi, F.; Ch. Paar; Leising, G.; Scherf, U.; Muellen, K.; Fischer, W.; Stelzer, F. *Mol. Cryst. Liq. Cryst.* **1994**, *256*, 549.

(4) Leising, G.; Tasch, S.; Graupner, W. In *Handbook of Conducting Polymers*, 2nd ed.; Marcel Dekker: New York, 1997; p 847.

(5) Tasch, S.; Brandstaetter, C.; Meghdadi, F.; Leising, G.; Athouel, L.; Froyer, G. *Adv. Mater.* **1997**, *9*, 33.

(6) Ambrosch-Draxl, C.; Majewski, J. A.; Vogl, P.; Leising, G. *Phys. Rev B* **1995,** *51*, 9668.

(7) Niko, A.; Meghdadi, F.; Ambrosch-Draxl, C.; Vogl, P.; Leising, G. *Synth. Met.* **1996**, *76*, 177.

(8) Zojer, E.; Knupfer, M.; Resel, R.; Meghdadi, F.; Leising , G.; Fink, J. *Phys. Rev. B* **1997**, *56*, 10 138.

(9) Era, M.; Tsutsui, T.; Saito, S. *Appl. Phys. Lett.* **1995**, *67*, 2436.

(10) See: Piaggi, A.; Lanzani, G.; Bongiovanni, G.; Mura, A.; Graupner, W.; Meghdadi, F.; Leising, G. *Phys. Rev. B* **1997**, *56*, 10 133. Graupner, W.; Meghdadi, F.; Leising, G.; Lanzani, G.; Nisoli, M.; De Silvestri, S.; Fischer, W.; Stelzer, F. *Phys. Rev. B* **1997**, *56*, 10 128, and refs therein.

(11) Cornil, J.; Santos, dos D. A., Crispin, X.; Silbey, R.; Bredas, J. L. *J. Am. Chem. Soc.* **1998,** *120*, 1289.

(12) Tasch, S.; Niko, A.; Leising, G.; Scherf, U. *Appl. Phys. Lett.* **1996**, *68*, 1090.

(13) Yang, Y.; Pei, Q.; Heeger, A. *Appl. Phys. Lett.* **1996**, *79*, 934.

(14) Loi, M. A.; List, E. J. W.; Gadermaier, C.; Graupner, W.; Leising, G.; Bongiovanni, G.; Mura, A.; Pireaux, J.-J.; Kaeriyama, K. *Synth. Met.* **2000**, *111*, 521.

(15) Rumi, M.; Zerbi, G. *Chem. Phys.* **1999**, *242*, 123.

(16) Bastiansen, O. *Acta Chem. Scand.* **1949**, *3*, 408.

(17) Tsuzuki, S.; Tanabe, K. *J. Phys. Chem*. **1991**, *95*, 139.
(18) Baker, K. N.; Fratini, A. V.; Resch, T.; Knachel, H. C.; Adams, W. W.; Socci, E. P.; Farmer, B. L. *Polymer* **1993**, *34*, 1571.
(19) Hertel, E.; Roemer, G. H. *Z. Phys. Chem*. B **1933**, *21*, 292; Hertel, E.; Roemer, G. H. *Z. Phys. Chem*. B **1933**, *23*, 226.
(20) Charbonneau, G. P.; Delugeard, Y. *Acta Crystallogr. B* **1977**, *33*, 1586.
(21) Baudour, J. L.; Cailleau, H.; Yelon, W. B. *Acta Crystallogr. B* **1977**, *33*, 1773.
(22) Delugeard, Y.; Desuche, J.; Baudour, J. L. *Acta Crystallogr. B* **1976**, *32*, 702.
(23) Hengstenberg, J.; Mark, H. *Z. Krist*. **1929**, *70*, 283.
(24) Rietveld, H. M.; Maslen, E. N.; Clews, C. J. B. *Acta Crystallogr. B* **1970**, *26*, 693.
(25) Trotter, J. *Acta Crystallogr*. **1961**, *14*, 1135.
(26) Bolognesi, A.; Catellani, M.; Destri , S.; Porzio, W. *Polymer* **1985**, *26*, 1628.
(27) Sasaki, S.; Yamamoto, T.; Kanbara, T.; Morita, A.; Yamamoto, J. *J. Polym. Sci. B* **1992**, *30*, 293.
(28) Socci, E. P.; Farmer, B. L.; Adams, W. W. J. *Polym. Sci. B* **1993**, *31*, 1975.
(29) Schön, J. H.; Chapter Kloc; Dodabalapur, A.; Batlogg, B. *Science* **2000**, *289*, 599.
(30) Clark, G. L.; Pickett, L. W. *Proc. Nat. Acad. Sci*. **1930**, *16*, 20.
(31) Desiraju, G. R.; Gavezotti, A. *Acta Crystallogr. B* **1989**, *45*, 473.
(32) Stevens, B. *Spectrochim Acta*. **1962**, *18*, 439.
(33) Toussaint, C.; Vos, G. *J. Chem. Soc. (B)* **1966,** 813.
(34) Toussaint, C. *Acta Crystallogr*. **1966**, *21*, 1002.
(35) *International Tables of X-ray Crystallography Vol. III, Physical and Chemical Tables*; Lonsdale, K., Reidel, D., Eds.; Dordrecht 1983.
(36) Carreira, L. A.; Towns, T. G. *J. Mol. Struct*. **1977**, *41*, 1.
(37) Kraus, W.; Nolze, G. *J. Appl. Cryst*. **1996**, *29*, 301.
(38) Athouël, L.; Froyer, G.; Riou, M. T.; Scott, M. *Thin Solid Films* **1996**, *274*, 35.
(39) Resel, R.; Koch, N.; Meghdadi, F.; Leising, G.; Unzog, N.; Reichmann, K. *Thin Solid Films* **1997**, *305*, 232.
(40) Zannoni, G.; Zerbi, G. *J. Chem. Phys*. **1985**, *82*, 31.
(41) Cuff, L.; Kertesz, M. *Macromolecules* **1994**, *27*, 762.
(42) Krichene, S.; Lefrant, S.; Froyer, G.; Maurice, F.; Pelous, Y. *J. De Physique* **1983**, *44*, C3−733.
(43) Furukawa, Y.; Ohtsuka, H.; Tasumi, M. *Synth. Met.* **1993**, *55*, 516.
(44) Rumi, M.; Zerbi, G.; Müllen, K.; Müller, G. *J. Chem. Phys*. **1997**, *106*, 1.
(45) Louarn, G.; Athouël, L.; Froyer, G.; Buisson, J. P.; Lefrant, S. *Synth. Met*. **1993**, *55*, 4762.
(46) Leising, G.; Verdon, T.; Louarn, G.; Lefrant, S. *Synth. Met*. **1991**, *41*, 279.
(47) Cuff, L.; Cui, C.; Kertesz, M. *J. Am. Chem. Soc*. **1994**, *116*, 9269.
(48) Yamamoto, T.; Yamamoto, A.; *Chem. Lett.* **1977,** 353.
(49) Baudour, J. L.; Delugeard, Y.; Rivet, P. *Acta Crystallogr*. B **1978**, *34*, 625.
(50) Cailleau, H.; Baudour, J. L.; Zeyen, C. M. E. *Acta Crystallogr*. B **1979**, *35*, 426.
(51) Cailleau, H.; Dworkin, A. *Mol. Cryst. Liq. Cryst*. **1979**, *50*, 21.
(52) For a biphenyl molecule the potential function governing internal rotations is given by a simple form in ref. (36).
(53) Häfelinger, G.; Regelmann, C. *J. Compt. Chem*. **1985**, *6*, 368.
(54) Mannfors, B.; Pietilä, L.-O.; Palmö, K. *J. Mol. Struct*. **1984**, *328*, 287.
(55) Webster, S.; Batchelder, D. N. *Polymer* **1996**, *37*, 4961.
(56) Born, M.; Huang, K. *Dynamical Theory of Crystal lattices*; Oxford University Press: Oxford, 1954; pp 38−40.
(57) Landolt-Börnstein *Zahlenwerte und Funktionen aus Physik, Chemie, Astronomie, Geophysik und Technik*; Springer, Berlin, 1957, 6th ed., Vol. 2.
(58) Yang, S.; Graupner, W.; Guha, S.; Puschnig, P.; Martin, C.; Chandrasekhar, H. R.; Chandrasekhar, M.; Leising, G.; Draxl, C.-A.; Scherf, U. *Phys. Rev. Lett.* **2000**, *85*, 2388.
(59) Heller, C.; Leising, G.; Gordon, C.; Lefrant, S.; Fischer, W.; Stelzer, F. *Phys. Rev B* **1995**, *51*, 8107.
(60) Frisch, M. J.; Trucks, G. W.; Schlegel, H. B.; Gill, P. M. W.; Johnson, B. G.; Robb, M. A.; Cheeseman, J. R.; Keith, T.; Petersson, G. A.; Montgomery, J. A.; Raghavachari, K.; Al-Laham, M. A.; Zakrzewski, V. G.; Ortiz, J. V.; Foresman, J. B.; Cioslowski, J.; Stefanov, B. B.; Nanayakkara, A.; Challacombe, M.; Peng, C. Y.; Ayala, P. Y.; Chen, W.; Wong, M. W.; Andres, J. L.; Replogle, E. S.; Gomperts, R.; Martin, R. L.; Fox, D. J.; Binkley, J. S.; Defrees, D. J.; Baker, J.; Stewart, J. P.; Head-Gordon, M.; Gonzalez, C.; Pople, J. A. Gaussian 94, Revision C.3. Gaussian Inc.: Pittsburgh, PA. 1995.
(61) Hehre, W. J.; Radom, L.; Schleyer , Paul v. R.; Pople J. A. *Ab Initio Molecular Orbital Theory*; John Wiley & Sons: New York, 1986.
(62) Becke, A. D. *J. Chem. Phys*. **1993**, *98*, 5648.
(63) Pulay, P.; Forgarasi, G.; Boggs, J. E.; Vargha, A. A. *J. Am. Chem. Soc*. **1983**, *105*, 7047.
(64) Irle, S.; Lischka, H. *J. Mol. Struct. (THEOCHEM)* **1996**, *364*, 15.
(65) Cui, C. X.; Kertesz, M. *J. Chem. Phys*. **1990**, *93*, 5257.